

Extracting oscillating components from nonstationary time series: A wavelet-induced method

Adrien Delière* and Samuel Nicolay

Department of Mathematics, University of Liège, Liège, Belgium

(Received 6 February 2017; published 11 September 2017)

This paper consists in the description and application of a method called wavelet-induced mode extraction (WIME) in the context of time-frequency analysis. WIME aims to extract the oscillating components that build amplitude modulated-frequency modulated signals. The essence of this technique relies on the successive extractions of the dominant ridges of wavelet-based time-frequency representations of the signal under consideration. Our tests on simulated examples indicate strong decomposition and reconstruction skills, trouble-free handling of crossing trajectories in the time-frequency plane, sharp performances in frequency detection in the case of mode-mixing problems, and a natural tolerance to noise. These results are compared with those obtained with empirical mode decomposition. We also show that WIME still gives meaningful results with real-life data, namely, the Oceanic Niño Index.

DOI: [10.1103/PhysRevE.96.033307](https://doi.org/10.1103/PhysRevE.96.033307)**I. INTRODUCTION**

Extracting the intrinsic components that constitute a given amplitude modulated-frequency modulated (AM-FM) signal is undoubtedly a subject of primary importance in many areas involving signal processing and analysis. Among the multiple benefits of such decompositions, one can mention that it allows us to better understand the underlying mechanisms governing the signal, to extract its main frequencies and their temporal variations, and to rule out noisy parts or irrelevant information for the study carried out. These aspects are generally encapsulated in a time-frequency (TF) representation of the signal and/or of the extracted components, which helps visualize the information contained in the signal from a time, energy, and frequency point of view simultaneously [1].

One of the most popular ways to tackle such a task is the well-known empirical mode decomposition (EMD; see, e.g., Refs. [2–4]). It is a complete adaptive fully data-driven algorithm that decomposes a signal into “intrinsic mode functions” (IMFs) that are, roughly speaking, AM-FM signals with slowly time-varying amplitudes and frequencies (i.e., they can be viewed as locally harmonic [5]). EMD has proven its effectiveness in many situations (such as medicine [6,7], climatology [8], finance [9], and geophysics [10]) despite its lack of mathematical background, which is often mentioned as its main drawback [5,11]. Moreover, by using EMD, one has little control over the results since no parameter can be tuned in this rather hermetic heuristic algorithm. Even though it has been shown to act as an adaptive filter bank [2] and many other studies have investigated its properties, methods that can be analytically described are also needed.

Wavelets are now well-established tools for signal analysis; their range of applications includes DNA analysis [12], acoustics [13], geology [14], climatology [15–17], and physiology [18,19], to name just a few. Wavelet transforms are provided with a rather strong mathematical theoretical background and with an inverse transform, which is the backbone of reconstruction procedures (see, e.g., Refs. [5,20,21]). However, in the classic continuous wavelet transform (CWT) analysis, all (or, in practice, many) wavelet

coefficients are needed to accurately rebuild the original signal, and the area of the TF plane needed for the reconstruction has to be manually selected (as in, e.g., Refs. [5,14]). Approaches such as in Ref. [22] resolve that problem by giving an automated way to determine which wavelet coefficients to use, but it appears that this method is relatively rigid and cannot deal with close frequencies nor with nonstationary signals. Other techniques such as in Ref. [11] consist in performing a segmentation of the Fourier spectrum of the signal in order to isolate the highest local maxima and then build a wavelet-basis associated with each so-obtained segment. Some kind of inverse wavelet transform allows the extraction of a component per segment. The results presented in Ref. [11] are interesting and the idea of segmenting the Fourier domain is appealing, but it turns out that the procedure described is rather complicated and is not well suited for the analysis of, e.g., “highly” nonstationary signals having an “erratic” Fourier spectrum. Let us also mention works such as Ref. [13], in which some curves called “skeletons” are extracted from the wavelet transform by considering stationary points in the “time-phase” plane that satisfy some properties. The idea is interesting as well, but it does not necessarily lead to components that can be viewed as signals (i.e., functions of time).

In this paper, we develop a wavelet-based mode decomposition that we call wavelet-induced mode extraction (WIME). This method aims to extract automatically signal-length AM-FM components that are present in a signal. It is inspired by some of the above-mentioned techniques and attempts to resolve most of their problems. The rest of this work is organized as follows. We first explain the concepts and the main ideas that animate WIME, before describing the algorithm in detail. We then apply WIME to synthetic signals that illustrate its advantages over the other methods, and we compare its skills with EMD, test its tolerance to noise, and discuss the results. Finally, we apply it to a real-life signal, the Oceanic Niño Index (ONI), and draw some conclusions. It is important to keep in mind that, even if WIME overcomes the problems encountered by EMD in some very specific cases (e.g., when the target components are not “well separated”), EMD remains a simple and efficient multipurpose technique in time-frequency analysis. This is the reason why such a standard bearer was naturally chosen as reference to assess our results.

*adrien.deliege@ulg.ac.be

II. WAVELET-INDUCED MODE EXTRACTION

In this section we first give the intuitive ideas that relate to WIME before going into further details. As a preliminary remark, one has to be aware of the class of functions that can be handled while developing a specific tool for signal analysis. Without going into technical details, we aim to deal with real-valued AM-FM signals of the type

$$f(t) = \sum_{k=1}^K a_k(t) \cos[\phi_k(t)],$$

defined on \mathbb{R} , where $a_k(t) > 0$, $\phi_k'(t) = d\phi_k(t)/dt > 0$ and $a_k(t)$, $\phi_k(t)$ are “smooth” (see, e.g., Ref. [5] for more technical details). It is clear that this class of functions is relatively large and that many real-life signals can be (at least partly) approximated by AM-FM components, even though pre- or post-processing treatments may be required.

A. The continuous wavelet transform

First, we briefly give the minimal mathematical notions required for a proper understanding of WIME; more information on the theoretical properties of wavelets can be found in the seminal works [20,21,23,24]. Given a wavelet ψ , the CWT of a function $f \in L^2(\mathbb{R})$ at position or time t and at scale $a > 0$ is defined as

$$W_f(t, a) = \int_{\mathbb{R}} f(x) \bar{\psi}\left(\frac{x-t}{a}\right) \frac{dx}{a}, \quad (1)$$

where $\bar{\psi}$ is the complex conjugate of ψ .

A wavelet ψ is called a progressive wavelet if its Fourier transform $\hat{\psi}$ satisfies $\hat{\psi}(\xi) = 0$ if $\xi \leq 0$. Progressive wavelets have the following convenient property [5]: If ψ is a progressive wavelet and if

$$f(t) = A \cos(\omega t + \varphi)$$

with $A, \omega > 0$, then

$$W_f(t, a) = \frac{A}{2} e^{i(\omega t + \varphi)} \overline{\hat{\psi}(a\omega)}. \quad (2)$$

In the context of time-frequency analysis, it is recommended to use a wavelet well located in the frequency domain [17,22]. In this work, as in Ref. [22], we use the Morlet-like wavelet ψ defined by its Fourier transform as

$$\hat{\psi}(\xi) = \sin\left(\frac{\pi\xi}{2\Omega}\right) e^{-\frac{-(\xi-\Omega)^2}{2}} \quad (3)$$

with $\Omega = \pi\sqrt{2/\ln 2}$, which is localized around Ω . In the time domain, we have

$$\psi(t) = \frac{e^{i\Omega t}}{2\sqrt{2\pi}} e^{-\frac{(2\Omega t + \pi)^2}{8\Omega^2}} \left(e^{\frac{\pi t}{\Omega}} + 1\right).$$

Since $|\hat{\psi}(\xi)| < 10^{-5}$ if $\xi \leq 0$, ψ can be considered as a progressive wavelet. Therefore, Eq. (2) holds and the choice of ψ [Eq. (3)] gives that, at any time t , the function

$$a \mapsto |W_f(t, a)| = \frac{A}{2} |\overline{\hat{\psi}(a\omega)}|$$

reaches its global maximum at a scale a^* that satisfies $a^* = \Omega/\omega$. As a consequence, if ω is unknown, it can be obtained

as $\omega = \Omega/a^*$. Besides, we have

$$W_f(t, a^*) = \frac{A}{2} e^{i(\omega t + \varphi)}.$$

The initial function f can thus be easily recovered from the real part of its CWT as

$$f(t) = 2\Re W_f(t, a^*) \quad (4a)$$

$$= 2|W_f(t, a^*)| \cos\{\arg[W_f(t, a^*)]\}. \quad (4b)$$

Now, if $f(t) = A(t) \cos(\phi(t))$, then around a given time t_0 one has

$$f(t) \approx A(t_0) \cos[\phi(t_0) + \phi'(t_0)(t - t_0)]$$

by truncated Taylor series [5]. If $a^*(t_0)$ denotes the scale at which $a \mapsto |W_f(t_0, a)|$ reaches its maximum, then the instantaneous frequency $\phi'(t_0)$ can be recovered from the fact that $a^*(t_0) = \Omega/\phi'(t_0)$ and Eq. (4) evaluated at t_0 and $a^*(t_0)$ gives back a value close to $f(t_0)$. Using the same process at each time t , AM-FM signals can be recaptured as

$$f(t) \approx 2|W_f(t, a^*(t))| \cos\{\arg[W_f(t, a^*(t))]\}.$$

As it can be seen below, this sole result propels WIME by itself.

B. Main ideas of the method

Basically, the first step of WIME is to perform a CWT of the signal as described above. The modulus of this CWT can be seen as a smooth TF representation of the signal. The wavelet spectrum is computed as

$$a \mapsto \Lambda(a) = E_t |W_f(t, a)|,$$

where E_t denotes the mean over time. Its global maximum is isolated and encapsulated in a frequency interval.

Then we choose a starting point with high energy in the TF plane in the selected time-frequency band and determine a ridge of high energy forward and backward from this point up to the edges of the plane while adapting the frequency window as we go along the ridge. A component modulated in amplitude and frequency by the modulus and argument of the CWT along that ridge can be extracted with Eq. (4) (i.e., two times the real part of the CWT along the ridge).

Finally, we subtract this component from the signal and repeat the whole process with this newly obtained signal. The procedure is iterated until the components extracted are no longer relevant.

Let us briefly comment some of the aspects of the proposed algorithm and contrast them with other methods. First, segmenting the wavelet spectrum instead of the Fourier spectrum (as in Ref. [11]) has the advantage of being easier since the wavelet spectrum is usually much smoother. For example, chirps will generally be handled comfortably with WIME while their Fourier spectra are extremely irregular and are therefore more difficult to segment. Also, unlike skeletons computed in Ref. [13], the ridges considered here can be viewed as functions of time and thus allow to derive signal-length components as desired, as EMD. Moreover, regarding Ref. [4], EMD extracts the IMFs of a signal one after another, sorting these by decreasing frequency. However,

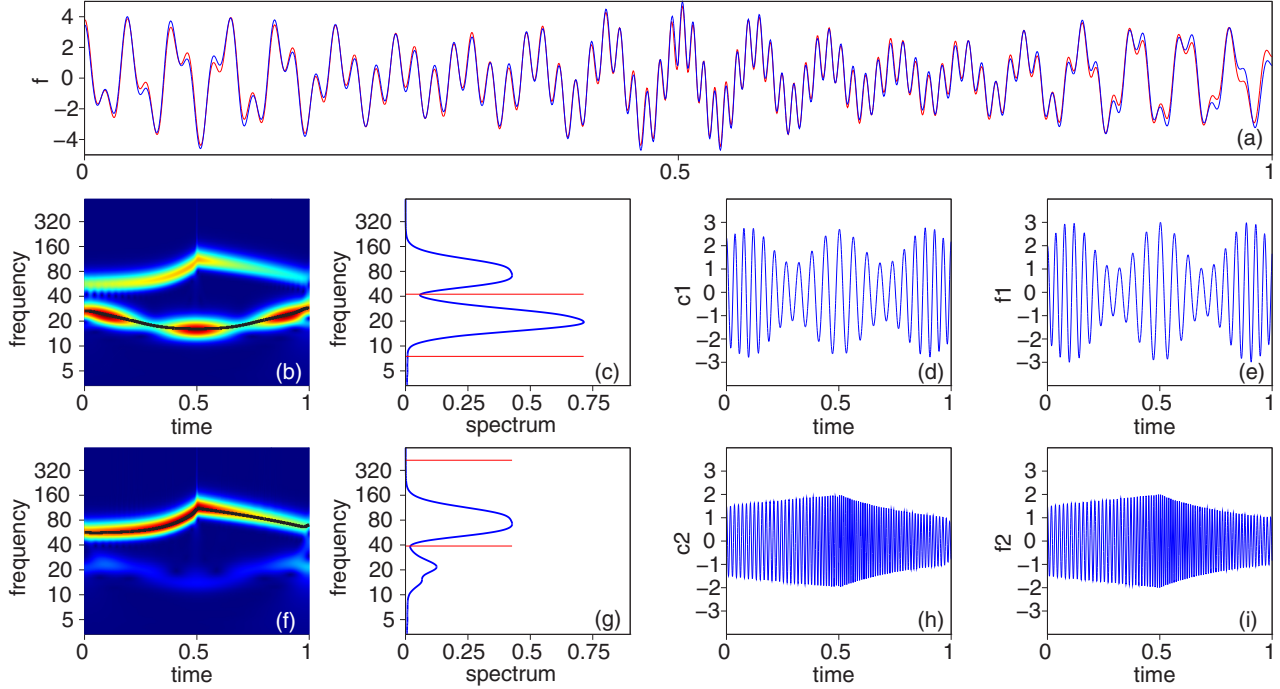


FIG. 1. (a) Original signal f (blue) and reconstructed signal (red) of Sec. III A; (b) $(t, a) \mapsto |W_f(t, a)|$ (stands for the TF representation of f) and ridge detected (black line); (c) wavelet spectrum of f and its segmentation (red lines) to isolate the highest local maximum (used to set a starting point for the ridge); (d) first component c_1 extracted following the ridge; (e) original first component f_1 ; figures (f) to (i) are the same figures with $f - c_1$ instead of f . Clearly, c_1 and c_2 successively extracted match f_1 and f_2 .

such an approach does not take into account the energetic hierarchical order of the components that build the signal. WIME resolves that problem by extracting the components successively by sorting them with respect to their energy level, starting with the most energetic ones. In this way, some kind of natural order is respected for the extraction, which is particularly useful when the TF representation of the signal displays, for example, intersecting curves.

C. Description of the algorithm

The algorithm of WIME applied on a signal f defined on a time interval T consists in the following steps:

- (1) Perform the CWT of f :

$$W_f(t, a) = \int_T f(x) \bar{\psi}\left(\frac{x-t}{a}\right) \frac{dx}{a}.$$

- (2) Compute the wavelet spectrum Λ associated with f :

$$a \mapsto \Lambda(a) = E_t |W_f(t, a)|,$$

where E_t denotes the mean over time.

- (3) Locate the scale a^* at which Λ reaches its highest local maximum and isolate it between the scales a_1 and a_2 at which Λ displays the left and right local minima that are the closest to a^* . Set $A = [a_1, a_2]$.

- (4) Define $(t_0, a(t_0))$ in the time-frequency band $T \times A$ of the TF plane as

$$(t_0, a(t_0)) = \underset{(t, a) \in T \times A}{\operatorname{argmax}} |W_f(t, a)|,$$

which is the starting point for the ridge detection step.

- (5) Compute¹ the ridge $(t, a(t))_{t \in T}$ forward and backward that stems from $(t_0, a(t_0))$:

- (a) Compute b_1 and b_2 such that $b_2 - b_1 = a_2 - a_1$ and $a(t_0) = (b_1 + b_2)/2$, i.e., center $a(t_0)$ in a frequency interval of the same length as the initial one.

- (b) Among the scales at which the function $a \in [b_1, b_2] \mapsto |W_f(t_0 + 1, a)|$ reaches a local maximum, define $a(t_0 + 1)$ as the closest one to $a(t_0)$. If there is no local maximum, then $a(t_0 + 1) = a(t_0)$.

- (c) Repeat step 5) with $(t_0 + 1, a(t_0 + 1))$ instead of $(t_0, a(t_0))$ until the end of the signal.

- (d) Proceed in the same way backward from $(t_0, a(t_0))$ until the beginning of the signal.

- (6) Extract the component associated with the ridge:

$$t \mapsto 2|W_f(t, a(t))| \cos[\arg W_f(t, a(t))].$$

- (7) Subtract this component (say c_1 at the first iteration) from f to get the rest $r_1 = f - c_1$ and repeat steps 1 to 7 with r_1 instead of f . Obtain c_2 , repeat with $r_2 = r_1 - c_2$, etc.

- (8) Stop the process (iterating steps 1 to 7) when enough energy has been drained from the signal. More precisely, if the components already extracted are denoted by $(c_i)_i$ for $i =$

¹For this step, keep in mind that we are working with signals, i.e., discrete time series and not functions defined on \mathbb{R} . We can thus move from “one point to the next,” i.e., the points located around t_0 can be considered as located at times $\dots, t_0 - 2, t_0 - 1, t_0 + 1, t_0 + 2, \dots$

$1, \dots, N$, then stop if

$$\left\| f - \sum_{i=1}^N c_i \right\| < \alpha \|f\|,$$

where we set the threshold $\alpha = 0.05$ and $\|\cdot\|$ denotes the energy of a signal from the signal analysis point of view (i.e., as the square of the L^2 norm).

The so-obtained components successively extracted are the counterparts of the IMFs from EMD and their sum provides an accurate reconstruction of f . The signal $c_0 = f - \sum_{i=1}^N c_i$ is considered as the remaining “noise,” and therefore the decomposition of f can be completed with this component, i.e., $f = \sum_{i=0}^N c_i$. Let us note that the ridge extraction can be made more difficult if many components of similar energy and frequency are added together within the signal. To overcome these difficulties, reallocation methods [25–27] such as synchrosqueezing [5,28] that sharpen the TF representation of the signal might be useful before the computation of the ridge.

TABLE I. Comparison of the extraction and reconstruction skills of WIME and EMD for the signal used in Sec. III A. The signal s_n corresponds to the n th component c_n (displayed in Fig. 1) in the case of WIME and to the n th IMF in the case of EMD. The last line compares the initial signal f and the reconstructed signal f_r defined as the sum of the components s_n related to each case.

Signals	WIME		EMD	
	RMSE	PCC	RMSE	PCC
s_1, f_1	0.261	0.987	0.163	0.995
s_2, f_2	0.070	0.998	0.171	0.989
f_r, f	0.267	0.991	0.151	0.997

III. EXPERIMENTS

A. Basic example

We now apply WIME on several signals in order to prove its effectiveness in various situations and depict some of its properties. We also compare its performances with EMD. For that purpose, the first example illustrates how WIME actually works. We consider the function $f = f_1 + f_2$ defined on $[0, 1]$

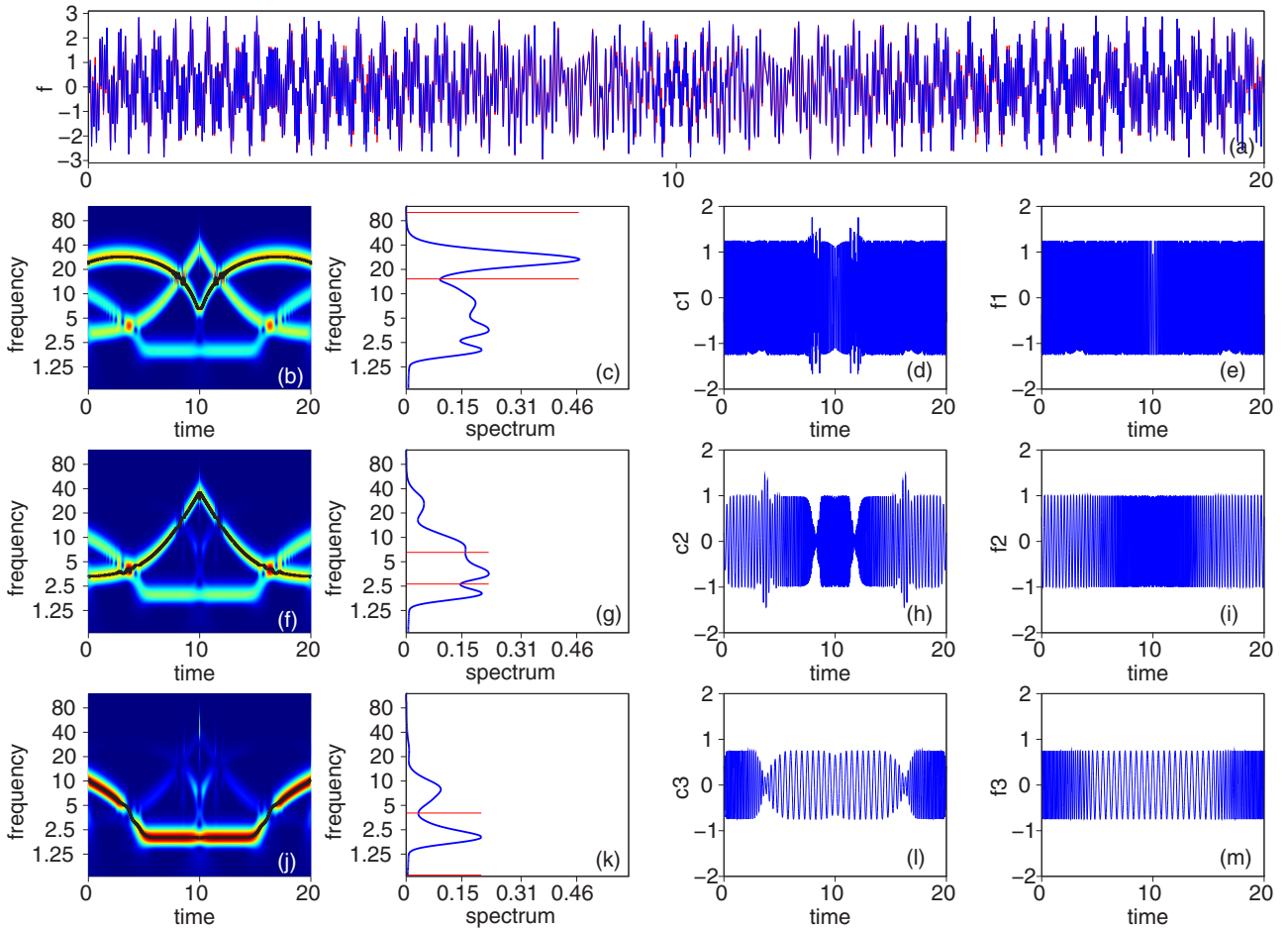


FIG. 2. As for Fig. 1, (a) displays the original signal f (blue) and the reconstructed one (red) of Sec. III B, and the other rows are, for the successive signals under consideration: (b), (f), (j) $|W_f(t, a)|$ and ridges (black line); (c), (g), (k) wavelet spectra; (d), (h), (l) components extracted following the ridges; (e), (i), (m) original components. The influence of the multiple crossings in the TF plane remains limited because WIME respects the energy-based hierarchical order of the components.

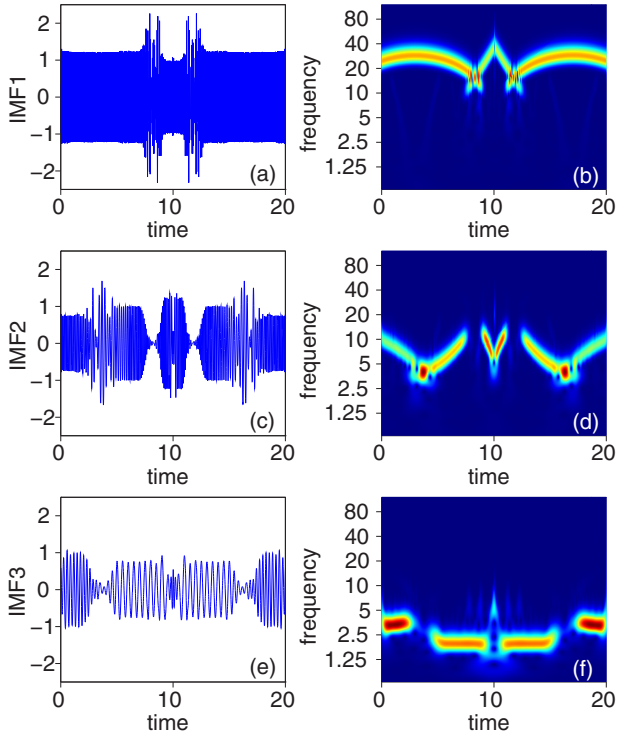


FIG. 3. (a), (c), (e) IMFs extracted with EMD from the signal of Sec. III B; (b), (d), (f) their TF representation obtained with the CWT. It can be seen that EMD works following a decreasing-frequency based approach, regardless the amplitudes of the components or IMFs to be extracted. Consequently, the IMFs only match the original components piecewise.

as the sum of two AM-FM components:

$$f_1(t) = (2 + \sin(5\pi t)) \cos[100(t - 0.5)^3 + 100t],$$

$$f_2(t) = \begin{cases} (1.5 + t) \cos(0.2e^{10t} + 350t) & \text{if } t \leq 0.5 \\ t^{-1} \cos(-300t^2 + 1000t) & \text{if } t > 0.5. \end{cases}$$

The signal and the steps of WIME applied to f are represented in Fig. 1. One can see that the first TF representation [i.e., $(t, a) \mapsto |W_f(t, a)|$] shows very distinctly the bricks used to build f . At the first step, the wavelet spectrum displays more energy (highest peak) around the 20 Hz frequency. The component c_1 extracted in that region corresponds to f_1 . At the next step, only the footprint of f_2 remains in the TF plane; the corresponding component c_2 matches with f_2 . Naturally, the reconstruction of f because of c_1 and c_2 is highly accurate, as shown in Fig. 1. Quantitative measurements through root mean square error (RMSE) and Pearson correlation coefficient (PCC) of the extraction and reconstruction skills of WIME and of EMD can be found in Table I. It appears that both methods display excellent skills, as expected for this basic example.

B. Crossings in the TF plane

For the next example, we consider a function made of three FM signals whose TF representations display some crossings and with constant amplitudes of 1.25, 1, 0.75. We consider

TABLE II. Extraction and reconstruction skills of WIME for the signal used in Sec. III B, with the same notations as previously. In this case, since the components are not recovered by EMD, the comparison is possible only with the reconstructed signal.

Signals	WIME		EMD	
	RMSE	PCC	RMSE	PCC
s_1, f_1	0.156	0.984	N/A	N/A
s_2, f_2	0.193	0.962	N/A	N/A
s_3, f_3	0.131	0.970	N/A	N/A
f_r, f	0.111	0.996	0.133	0.994

$f(t) = f_1(t) + f_2(t) + f_3(t)$ for $t \in [0, 10]$ with

$$f_1(t) = 1.25 \cos[-(t - 3)^3 + 180t],$$

$$f_2(t) = \cos(1.8^t + 20t),$$

$$f_3(t) = \begin{cases} 0.75 \cos(-1.6\pi t^2 + 20\pi t) & (t < 5) \\ 0.75 \cos(4\pi t) & (t \geq 5) \end{cases},$$

and we then set $f(10 + t) = f(10 - t)$ for every $t \in [0, 10]$ (i.e., f is concatenated with its mirror).

The TF representation of this signal displays, as wanted, multiple crossings between the patterns associated with each component (see Fig. 2). However, as it can be seen in Fig. 2, the energy corresponding to each component allows WIME to successfully retrieve the original components; the influence of the crossings remains extremely low. Naturally, when a crossing occurs, WIME follows the “first come, first served” principle: the energy is consumed by the first component that has the crossing on its way, and when another component reaches that point, there is no energy left for it even though it should have been the case. This phenomenon can be noticed in Fig. 2 and is unavoidable without treating or adjusting a component before extracting the next one. Nevertheless, the components obtained respect the hierarchical order imposed by their energy level and remain easily interpretable from a physical point of view.

This example also shows how EMD proceeds to extract successive components, and why it is not well adapted in that type of case. The EMD acts as a bandpass filter [2], filtering components following a frequency-decreasing order, i.e., high-frequency IMFs are extracted first, regardless their energy level. From a TF representation perspective, this corresponds to successively extract components related to the “upper ridge” present in the considered signal, then subtracting it, extracting the next “upper ridge,” and so on. This is illustrated in Fig. 3, which displays the first three IMFs obtained with EMD from f and their CWT-based TF representation.² This also depicts why EMD has such effective reconstruction skills: at the end of the process, as for WIME, all the energy of the TF plane has been drained, ridge after ridge. This can be seen in Table II,

²The TF-representation of the IMFs extracted from EMD is generally performed with the Hilbert transform [3], but we use the CWT to facilitate comparison with the other signals analyzed in this paper.

which displays the skills of the methods. The problem lies in the fact that the hierarchical order imposed by the amplitudes of the three components is not respected at all with EMD, which thus gives IMFs that are not as easily interpretable from a physical point of view. Even though it is probably useful to have such a filtering approach in some cases (e.g., for denoising purposes), something is clearly wrong in this case. Besides, EMD has no choice but following that order of filtering whereas WIME is more flexible and could be adapted to perform a similar task if needed.

C. Mode-mixing problem

The first example shows that WIME successfully retrieves components that are “well-separated” in the TF plane, where

the intuitive conditions to be “well separated” (avoiding crossings) could be defined with frequency-based formulas as in Ref. [5]. The second signal shows that when the components are not “well separated” with respect to their frequencies but are distinguishable by their amplitudes, then WIME still manages to recover the original sources of the signal, while EMD cannot. It is thus natural now to address the mode-mixing problem that occurs when a signal is made of AM-FM components that are relatively close to each other, i.e., the components are not “well separated” with respect to their frequency nor with their amplitudes. In this example, we still aim to obtain a satisfying recovery of the initial components, but we also want an accurate detection of the associated main frequencies. The signal f considered for that purpose is made of one AM-FM component and three AM components (t takes

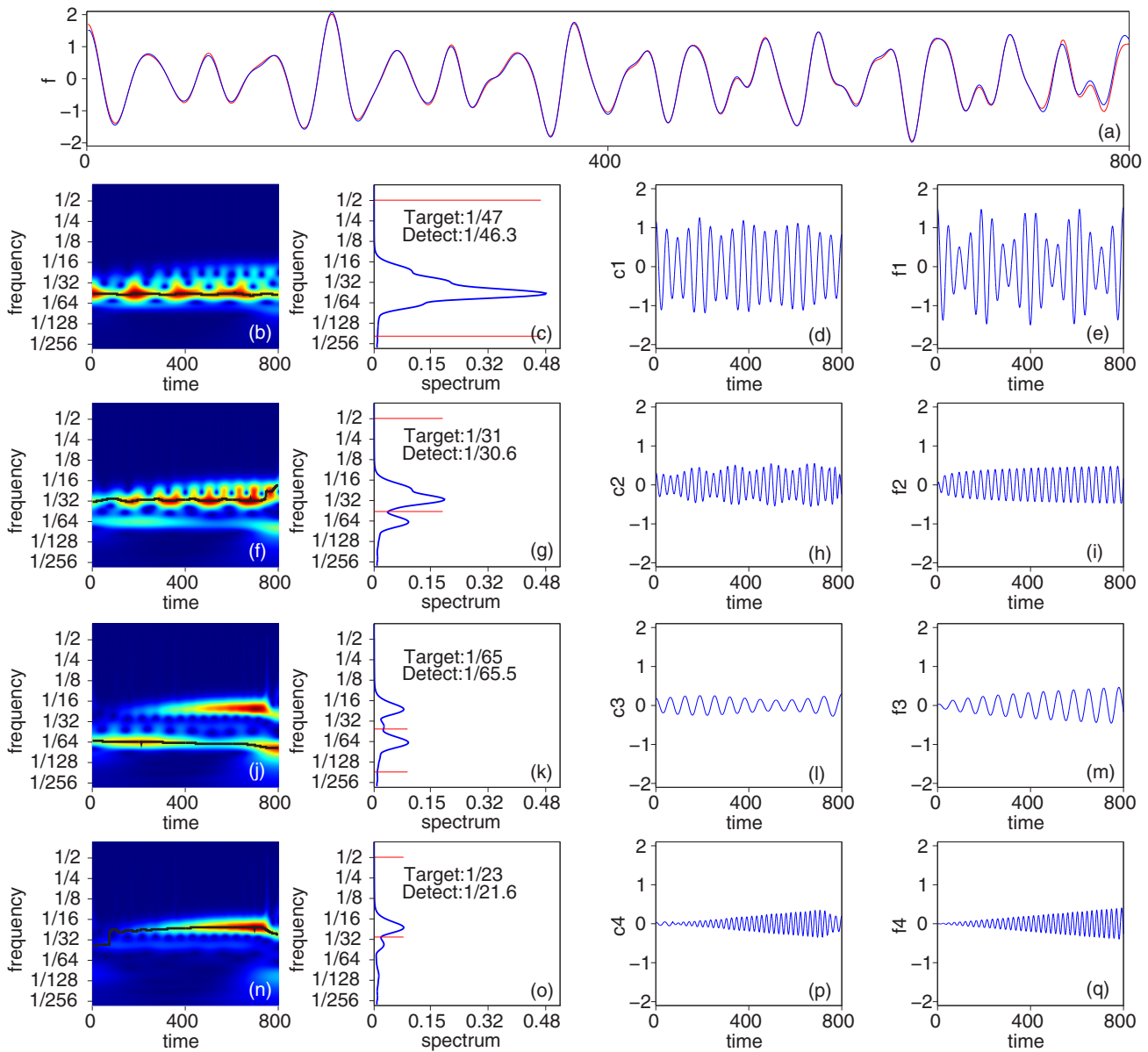


FIG. 4. As previously, (a) displays the original signal f (blue) and the reconstructed one (red) (Sec. III C); the other rows are, for the successive signals under consideration: (b), (f), (j), (n) $|W_f(t,a)|$ and ridges (black line); (c), (g), (k), (o) wavelet spectra; (d), (h), (l), (p) components extracted following the ridges; (e), (i), (m), (q) original components. The period detection skill of WIME is high.

integer values from 1 to 800):

$$f_1(t) = \left[1 + 0.5 \cos\left(\frac{2\pi}{200}t\right) \right] \cos\left(\frac{2\pi}{47}t\right),$$

$$f_2(t) = \frac{\ln(t)}{14} \cos\left(\frac{2\pi}{31}t\right),$$

$$f_3(t) = \frac{\sqrt{t}}{60} \cos\left(\frac{2\pi}{65}t\right),$$

$$f_4(t) = \frac{t}{2000} \cos\left[\frac{2\pi}{23 + \cos\left(\frac{2\pi}{1600}t\right)}t\right],$$

so that the target frequencies to detect are, respectively, 1/47, 1/31, 1/65, and $\approx 1/23$ Hz.

A peculiarity of this example is that the first component dominates the signal (see Fig. 4), with a mean energy much higher than the others. This has the effect of eclipsing the other components at first sight, and, looking at the first wavelet spectrum, it is complicated to tell which frequencies are present in the signal. In the case of WIME though, the successive subtractions of the components unveil the less powerful ones, as shown in Fig. 4, and so allow to detect almost exactly the target frequencies. The fact that hidden information may appear when dominant modes are correctly identified and taken off the signal may be useful in real-life data analysis such as daily temperature signals with a dominant mode of 365 days. Therefore, even though the components retrieval is satisfying but not as accurate as in the previous examples, substantial information can still be obtained with WIME.

As for the previous section, EMD does not perform so well in this case. The first four IMFs extracted with EMD are represented in Fig. 5. While the components extracted

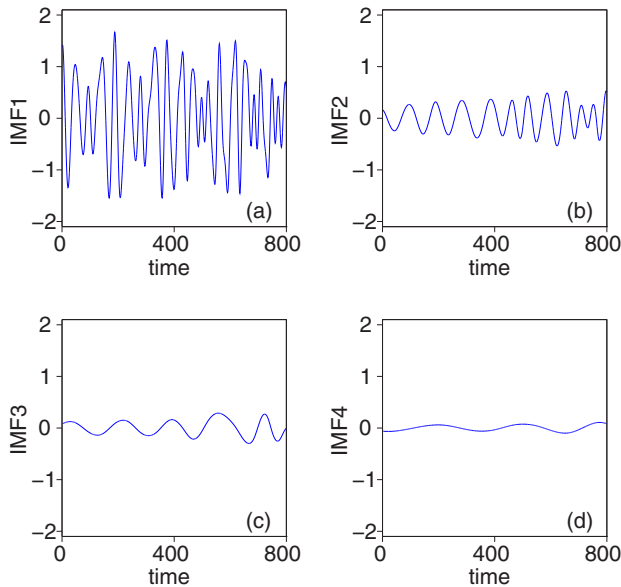


FIG. 5. IMFs obtained with EMD from the signal of Sec. III C. They are considerably different from the original components; the first IMF itself (a) represents almost the whole signal. The estimated frequencies [$\approx 1/41$ (a), $1/75$ (b), $1/165$ (c), $1/284$ (d) Hz] are far from the targets ($\approx 1/23, 1/31, 1/47, 1/65$).

TABLE III. Extraction and reconstruction skills of WIME for the signal used in Sec. III C. In the third line s_3^* corresponds to IMF₂ for EMD. The components are not recovered by EMD, the comparison is possible only in some cases.

Signals	WIME		EMD	
	RMSE	PCC	RMSE	PCC
s_1, f_1	0.205	0.962	0.458	0.831
s_2, f_2	0.109	0.932	N/A	N/A
s_3^*, f_3	0.170	0.694	0.259	0.462
s_4, f_4	0.070	0.902	N/A	N/A
f_r, f	0.064	0.997	0.068	0.998
f_1, f		RMSE:0.407	PCC:0.868	
s_1, f	0.392	0.878	0.316	0.926

with WIME are somehow close the real ones, with the target frequencies unquestionably recovered, the IMFs have nothing in common with the original components. With a PCC with f close to 0.93, the first IMF is almost the initial signal itself and with estimated frequencies of $\approx 1/41, 1/75, 1/165, 1/284$ Hz

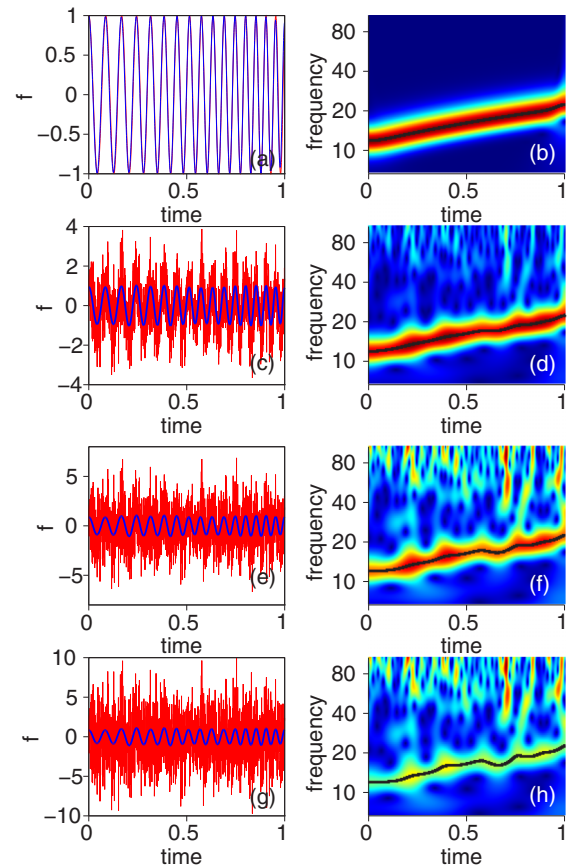


FIG. 6. (a) Original chimp (red) and extracted component (blue) associated with the ridge of the TF representation of the signal (b). Remaining rows: the same with $f + X$ (c), (d), $f + 2X$ (e), (f), $f + 3X$ (g), (h), where X is a Gaussian white noise with zero mean and variance 1. One can see that, despite the high level of noise, WIME is still able to retrieve the initial chimp. Moreover, it does not require any pre- or post-processing treatment or extra computational power.

TABLE IV. Reconstruction skills of WIME in the presence of noise ($f_r = c_1$).

Signals	SNR	RMSE	PCC
$f_r, f + X$	-2.792	0.129	0.983
$f_r, f + 2X$	-8.812	0.193	0.962
$f_r, f + 3X$	-12.330	0.263	0.929

(instead of $\approx 1/23, 1/31, 1/47, 1/65$), we can safely conclude that EMD fails the frequency detection test. As in the previous cases, a comparison of the skills of the methods is presented in Table III, which illustrates the nice performance of WIME compared to EMD.

D. Tolerance to noise

The next step consists in performing a resistance to noise test with WIME. Given the intrinsic nature of WIME, more precisely the CWT part which involves convolutions with a smooth kernel, it can be expected that WIME displays some kind of natural tolerance to noise. In the same spirit as in Ref. [5], we consider a chirp f defined on $[0, 1]$ by

$$f(t) = \cos(70t + 30t^2),$$

we generate a Gaussian white noise X of zero mean and variance 1, and we run WIME on f , $f + X$, $f + 2X$, and $f + 3X$. For the noisy signals $f + nX$ with $n > 0$, the corresponding signal-to-noise ratio (SNR) is defined as in Ref. [5] by

$$\text{SNR}[\text{dB}] = 10 \log_{10} \left[\frac{\text{var}(f)}{\text{var}(nX)} \right].$$

In the present case, the SNRs considered are respectively -2.792 , -8.812 , and -12.330 dB, indicating a particularly high level of noise in the last two cases. The results obtained on these noisy signals are displayed in Fig. 6. It can be noted that WIME successfully extracts f from the signals despite the high level of noise, especially in the third and fourth cases. This capacity is quantified more in detail in Table IV. It is important to note that such excellent results are obtained with no extra computational cost, i.e., WIME does not need to be adapted in any way to deal with noise. On the contrary, it is known that EMD has trouble to handle such erratic signals since it works in the time domain and is first concerned with high-frequency components, which is why we do not expand on that part. For the record, when performing EMD on $f + X$, the IMF which is the closer to f in terms of RMSE and PCC has a RMSE of 0.35 and a PCC of 0.869, which is much weaker than the results presented in Table IV. In this context, it would be preferable to use improved but time-consuming versions of this method

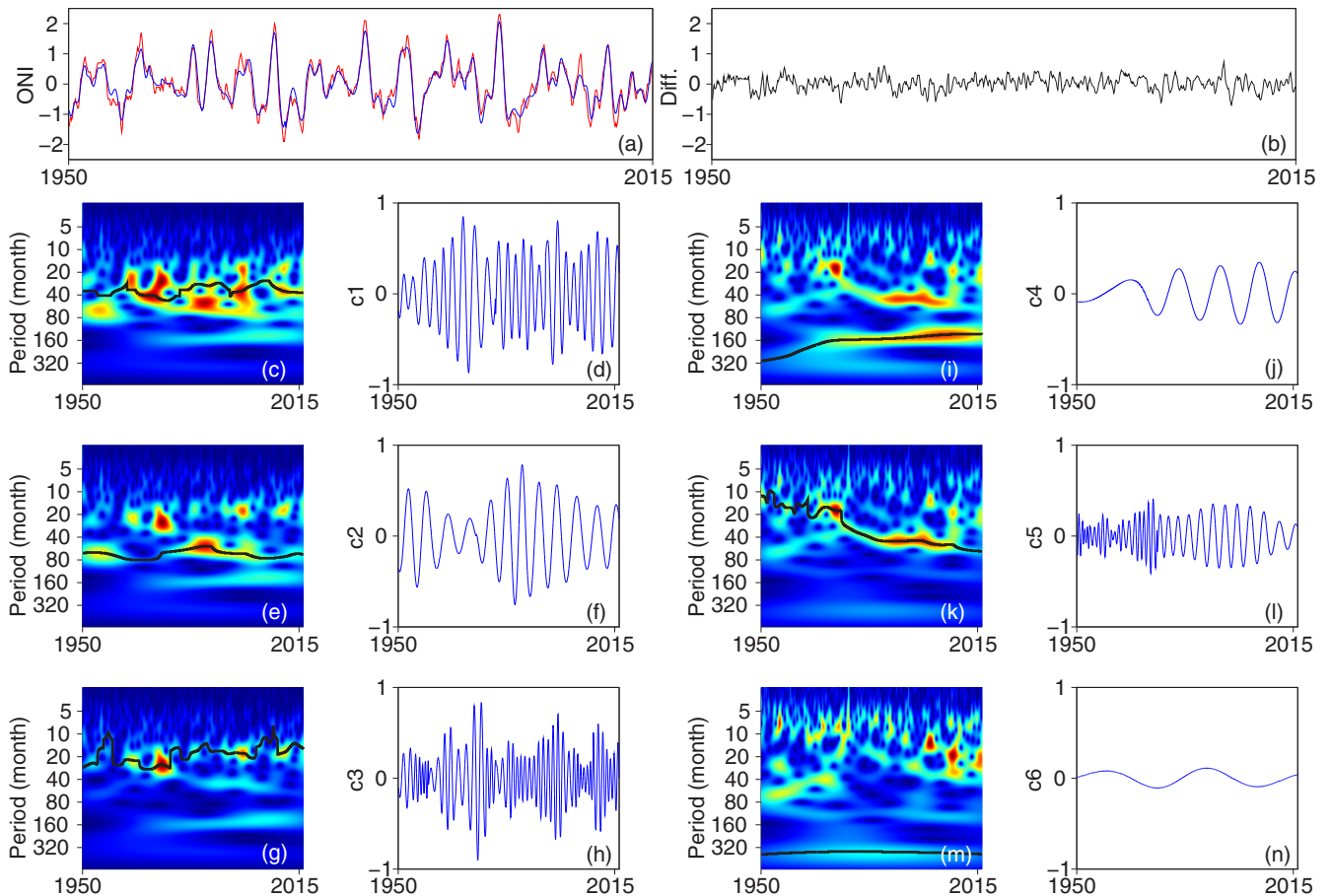


FIG. 7. (a) Original ONI signal (red) and reconstructed signal (blue); (b) the difference between them. Then the first six successive TF representations (c), (e), (g), (i), (k), (m) and components (d), (f), (h), (j), (l), (n) obtained with WIME.

such as the Ensemble Empirical Mode Decomposition [8] and the Complete Ensemble Empirical Mode Decomposition with Adaptive Noise [29]. Therefore, the natural tolerance to noise of WIME is part of its key assets.

E. Test on a real-life signal: ONI index

As a final test, we apply WIME on the ONI index, which is a 3-month running mean of sea surface temperature anomalies in the so-called Niño 3.4 area in the Pacific Ocean. At the Climate Prediction Center, ONI is the principal measure for monitoring, assessing, and predicting the well-known El Niño and La Niña events. This signal is of primary interest in climatology and is extensively studied (see, e.g., Refs. [16,17,30,31] and references therein).

The components extracted with WIME are presented in Fig. 7. It can be seen that WIME still gives satisfying results with this signal. Indeed, the components extracted have periods similar to those obtained in the literature (see Refs. [16,31] and references therein), ranging from near-annual to decadal modes of variability. The energy of the TF plane is drained so that the reconstruction appears smooth but accurate: the RMSE equals 0.22 and the PCC 0.96. We recall that these results are obtained with no pre- or post-processing treatment or adaptation of WIME; it is thus reasonable to assert that it can be used in the context of real-life data analysis. Let us finally add that WIME could help us improve our forecasts of ONI performed with the model presented in Ref. [16]; indeed, the ridges allow some desirable flexibility and could be used intelligently to derive excellent predictions of ONI.

IV. CONCLUSION

We introduced a new method within the framework of time-frequency analysis called wavelet-induced mode extraction (WIME), whose main purpose is to extract automatically the intrinsic components that form AM-FM signals. This technique borrows some characteristics of excellent mode decomposition procedures while trying to resolve some of their defects. The underlying philosophy consists in successively deriving components from high-energy ridges of the TF plane initiated by a segmentation of the wavelet spectrum.

When applied to toy examples, WIME displayed accurate decomposition skills. Indeed, the components retrieval involving nonstationary sources was carried out almost flawlessly. Compared to EMD, the results appeared as good in the simple cases and better in the trickier ones chosen here. As a matter of example, components that were well separated with respect to their amplitude but with intersecting trajectories in their TF representations were definitely recovered, while EMD failed to do so. Besides, when the focus was on the recapture of known frequencies in a mode-mixing problem, WIME outperformed EMD. It also appeared that the natural tolerance to noise of WIME makes it suitable to study natural time series. As a matter of example, the application to the ONI index showed that sound results are still obtained with real-life data.

As future work, we aim at developing WIME as much as possible, studying its properties in more detail and comparing its skills with many other techniques. It could also be worth trying to adapt WIME to wavelet-like methods such as the increasingly popular S transform [32,33], which displays some similarities with the CWT. Besides, WIME could be used in combination with other wavelet methods in the context of multifractal analysis, as has already been the case with EMD in, e.g., Refs. [34,35]. A particularly interesting example would be to use WIME in physiology along with the multifractal technique used in Refs. [18,19] for breast cancer detection. Roughly speaking, it appears that the physiological noise measured on thermograms has different multifractal properties in the presence of mammary glands with malignant tumors. An important step could be to use WIME to extract and study the variations of the dominant cardiac oscillatory components, which could bring complementary information about the diagnosis. The rest of the signal could also be used for finer analyses.

Finally, let us mention that a practical easy-to-use Scilab toolbox has been released³ so that nonspecialist researchers get to know better wavelets and time-frequency analysis, and can carry out their own mode decomposition experiments.

ACKNOWLEDGMENT

Funding was provided by the Fonds de la Recherche Scientifique de Belgique (F.R.S.-FNRS).

³https://atoms.scilab.org/toolboxes/toolbox_WIME/0.1.0

-
- [1] P. Flandrin, *Time-Frequency/Time-Scale Analysis, Wavelet analysis and Its applications* (Academic Press, London, 1999).
 - [2] P. Flandrin, G. Rilling, and P. Goncalves, *IEEE Signal Process. Lett.* **11**, 112 (2004).
 - [3] N. E. Huang, Z. Shen, S. R. Long, M. C. Wu, H. H. Shih, Q. Zheng, N.-C. Yen, C. C. Tung, and H. H. Liu, *Proc. R. Soc. London A* **454**, 903 (1998).
 - [4] G. Rilling, P. Flandrin, and P. Goncalves, in *IEEE-EURASIP Workshop Nonlinear Signal Image Processing (NSIP)* (2003).
 - [5] I. Daubechies, J. Lu, and H.-T. Wu, *J. Appl. Comput. Harmonic Anal.* **30**, 243 (2011).
 - [6] M. Costa, A. A. Priplata, L. Lipsitz, Z. Wu, N. Huang, A. Goldberger, and C.-K. Peng, *Europhys. Lett.* **77**, 68008 (2007).
 - [7] D. Cummings, R. Irizarry, N. Huang, T. Endy, A. Nisalak, K. Ungchusak, and D. Burke, *Nature (London)* **427**, 344 (2004).
 - [8] Z. Wu and N. E. Huang, *Adv. Adapt. Data Anal.* **1**, 1 (2009).
 - [9] N. Huang, M.-L. Wu, W. Qu, S. Long, S. Shen, and J. Zhang, *Appl. Stochastic Models Bus. Indust.* **19**, 245 (2003).
 - [10] N. E. Huang and Z. Wu, *Rev. Geophys.* **46**, RG2006(R) (2008).
 - [11] J. Gilles, *IEEE Trans. Signal Process.* **61**, 3999 (2013).
 - [12] A. Arneodo, C. Vaillant, B. Audit, F. Argoul, Y. d'Aubenton Carafa, and C. Thermes, *Phys. Rep.* **498**, 45 (2011).

- [13] G. Saracco, P. Guillemain, and R. Kronland-Martinet, *IEEE Ultrasonics* **2**, 881 (1990).
- [14] U. Gebhardt and M. Hiete, *Geol. Soc., London, Special Pub.* **376**, 177 (2013).
- [15] A. Deliège and S. Nicolay, *Pure Appl. Geophys.* **173**, 2885 (2016).
- [16] A. Deliège and S. Nicolay, *Pure Appl. Geophys.* **174**, 1815 (2017).
- [17] C. Torrence and G. Compo, *Bull. Am. Meteorol. Soc.* **79**, 61 (1998).
- [18] E. Gerasimova, B. Audit, S. G. Roux, A. Khalil, O. Gileva, F. Argoul, O. Naimark, and A. Arneodo, *Front. Physiol.* **5**, 176 (2014).
- [19] E. Gerasimova-Chechkina, B. Toner, Z. Marin, B. Audit, S. G. Roux, F. Argoul, A. Khalil, O. Gileva, O. Naimark, and A. Arneodo, *Front. Physiol.* **7**, 336 (2016).
- [20] I. Daubechies, *Ten Lectures on Wavelets* (SIAM, Philadelphia, 1992).
- [21] S. Mallat, *A Wavelet Tour of Signal Processing* (Academic Press, San Diego, 1999).
- [22] S. Nicolay, *Eur. Phys. J. B* **80**, 223 (2011).
- [23] S. Mallat, *Trans. Am. Math. Soc.* **315**, 69 (1989).
- [24] Y. Meyer and D. Salinger, *Wavelets and Operators* (Cambridge University Press, Cambridge, 1995), Vol. 1.
- [25] F. Auger and P. Flandrin, *IEEE Trans. Signal Proc.* **43**, 1068 (1995).
- [26] E. Chassande-Mottin, I. Daubechies, F. Auger, and P. Flandrin, *IEEE Signal Process. Lett.* **4**, 293 (1997).
- [27] E. Chassande-Mottin, F. Auger, and P. Flandrin, Time-frequency/time-scale reassignment, in *Wavelets and Signal Processing*, edited by L. Debnath (Birkhäuser, Boston, 2003), pp. 233–267.
- [28] I. Daubechies and S. Maes, *Wavelets in Medicine and Biology* (CRC Press, New York, 1996), pp. 527–546.
- [29] M. E. Torres, M. A. Colominas, G. Schlotthauer, and P. Flandrin, in *IEEE International Conference on Acoustic, Speech and Signal Processing (ICASSP)* (IEEE, Piscataway, NJ, 2011).
- [30] A. G. Barnston, M. K. Tippett, M. L. L’Heureux, S. Li, and D. G. DeWitt, *Bull. Am. Meteorol. Soc.* **93**, 631 (2012).
- [31] D. Petrova, S. J. Koopman, J. Ballester, and X. Rodó, *Climate Dyn.* **48**, 1249 (2017).
- [32] R. G. Stockwell, L. Mansinha, and R. P. Lowe, *IEEE Trans. Signal Proc.* **44**, 998 (1996).
- [33] S. Ventosa, C. Simon, M. Schimmel, J. J. Danobeitia, and A. Manuel, *IEEE Trans. Signal Proc.* **56**, 2771 (2008).
- [34] P. Caraianni, *PLoS ONE* **7**, 1 (2012).
- [35] G. S. Welter and P. A. A. Esquef, *Phys. Rev. E* **87**, 032916 (2013).